Design and characterisation of cantilevers for multi-frequency atomic force microscopy

Steven Ian Moore ✉, *Yuen Kuan Yong*

The School of Electrical Engineering and Computer Science, The University of Newcastle, Callaghan 2308, NSW, Australia
✉ *E-mail: steven.i.moore@uon.edu.au*

Published in Micro & Nano Letters; Received on 14th September 2016; Revised on 6th January 2017; Accepted on 23rd January 2017

The experimental characterisation of a set of microcantilevers targeted at use in multi-frequency atomic force microscope is presented. The aim of this work is to design a cantilever that naturally amplifies its harmonic oscillations which are introduced by nonlinear probe–sample interaction forces. This is performed by placing the modal frequencies of the cantilever at integer multiples of the first modal frequency. The developed routine demonstrates the placement of the frequency of the second to fifth mode. The characterisation shows a trend that lower-order modes are more accurately placed than higher-order modes. With two fabricated designs, the error in the second mode is at most 2.26% while the greatest error in the fifth mode is at 10.5%.

1. Introduction: Since the invention of atomic force microscope (AFM), it has emerged as one of the most versatile tools for interrogating and studying objects at the nanoscale [1, 2]. AFMs have contributed to breakthroughs in areas such as nanomachining [3], nanometrology [4], material science [5], semiconductor manufacturing [6] and high-density date storage systems [7].

An AFM uses a microcantilever, with an extremely sharp probe at its free end, to scan the surface of a sample. The probe–sample interaction forces cause the cantilever to deflect and this deflection is measured to observe the surface topography of the sample.

The need to study dynamic biological processes at high-speed and with low probe–sample interaction force (<1 nN) has led to the development of dynamic AFM [8]. Among many forms of dynamic AFM, tapping-mode is particularly attractive for imaging soft samples. The tapping cantilever vibrates at its resonance frequency, gently tapping the surface of a sample once per cycle. The vertical feedback loop is used to regulate its oscillation amplitudes. These oscillations are a function of the probe–sample force which in turn is dictated by the probe–sample separation. By compensating for those changes, the vertical feedback control signal can be used to generate high-resolution surface topography of the sample.

Despite the success of AFM, the technique currently faces limitation in terms of spatial resolution and quantitative measurements [9]. It is a challenging task to simultaneously obtain high-resolution topography and mapping of material properties (e.g. stiffness) on soft samples. This is due to the lack of sensitivity or difficulties in separating elastic information from the measured signal [10]. To overcome these difficulties, multi-frequency AFM methods have recently emerged as a new field in force microscopy [9]. Conventional dynamic AFM methods involve the excitation and detection of a single frequency component (usually the fundamental mode) of the cantilever's deflection. As a result, the information about the sample's properties that is encoded in the deflection at frequencies other than the excitation frequency is lost. Multi-frequency AFM methods involve the excitation and/or detection of several frequencies. Different resonances (modes) act as signal channels that provide access to different material properties including topography, elastic modulus and electrostatic and magnetic forces [11].

One approach to multi-frequency AFM is to use higher-order harmonics for imaging. The higher-order harmonic components of the cantilever's deflection are introduced due to the nonlinear probe–sample interaction forces. The amplitude of the harmonic vibrations decreases by $\sim 1/n$ (n is the order of harmonics) [9]. These small harmonic vibrations become difficult to detect.

To naturally amplify these harmonics, a number of researchers have designed harmonic probes/cantilevers whose modal frequencies lie at integer multiples of the fundamental frequency [12–16].

Initial design approaches parameterised the cantilever in terms of the dimensions of various topological features [12–14]. By systematically varying these parameters while performing modal analysis, a relationship between these parameters and the modal frequencies is formed. This approach heavily restricts the design space and limits the frequency placement to only a single mode.

A more flexible approach is to form a structure as set of finite elements (FEs) and, via an optimisation routine, vary properties or dimensions of the elements to design the cantilever. Cai *et al.* [16] split the cantilever into Euler–Bernoulli beam elements and optimisation sets the width of each element. The use of beam elements ignores torsional modes and only modifies the boundary of the cantilever, not the topology, restricting potential solutions. Xia *et al.* [15] apply the level set method to place the modal frequencies allowing for arbitrary two-dimensional (2D) topologies to be formed. However, only the placement of one modal frequency at a high-order harmonic (the 16th) is demonstrated. Furthermore, the curved topologies produced by the level set method are difficult to fabricate using microfabrication.

The non-convex mapping between the topology and the modal frequencies [17] presents an issue for the gradient-based optimisation used by Xia *et al.* [15] and Cai *et al.* [16]. For non-convex cost functions, gradient-based optimisation tends to converge to locally optimal solutions. Moreover, for complex cost functions and constraints, the definition of the gradient of the cost function is difficult to derive or does not exist.

This work develops a topology optimisation routine for an AFM cantilever. The aim of the optimisation routine is to place several modal frequencies at integer multiples of the fundamental frequency. The cantilever is modelled using the FE method and a genetic algorithm is used to form the topology of the cantilever. The proposed optimisation routine provides a number of benefits over existing routines for harmonic cantilever designs. It provides the flexibility to place multiple modal frequencies simultaneously. This work demonstrates the placement of four modes (the second to the fifth) at integer multiples of the first. This includes both flexural and torsional modes. The use of the genetic algorithm provides advantages over gradient-based-optimisation routines. The

genetic algorithm is a simple stochastic search that performs a global search, easily handles the complex relationship between the modal frequencies and the cantilever's topology and is well suited to handling the discrete variables that are used to represent the topology. The optimisation routine can produce arbitrary 2D topologies and the resulting designs are easily fabricated using microfabrication.

This Letter is organised as follows. Section 2 briefly outlines the process used to model the cantilever and performs modal analysis. Section 3 outlines how the cantilever topology is represented. Section 4 provides details of the genetic algorithm used to modify the topology to place the modal frequencies of the cantilever. Section 5 describes two designs that resulted from the execution of the optimisation routine. The cantilevers were fabricated and the experimental characterisation of the designs is presented in Section 6.

2. Mindlin plate theory and the FE method: Of concern in this work is the location of the modal frequencies of the AFM cantilever. Modelling only the elastic behaviour of a structure results in a conservative system in which harmonic solutions $x(t) = u\cos(\omega t)$ exist under no external force or load. The amplitude u is the mode shape with a modal frequency ω.

The cantilever is modelled using the Mindlin plate theory [18] to accurately account for arbitrary 2D topologies and to capture the torsional and plate modes that exist in AFM cantilevers [19]. The FE method [18, 20] is applied to analyse the structure.

The cantilever is discretised as a set of four node rectangular Mindlin plate elements. The nodes in the corners of the rectangular element are parameterised by three degrees-of-freedom: the deflection in the z-axis, rotation in the x-axis and rotation in the y-axis. The x and y axes are along the width and length of the plate, respectively, and the z-axis is along the thickness of the plate. For analysis of an individual element, the coordinate system of the element is mapped from (x, y) to (ξ, η) by placing the origin at the centre of the element and placing the nodes at coordinates $(-1, -1)$, $(1, -1)$, $(1, 1)$ and $(-1, 1)$. In the (ξ, η) coordinate system, the FE shape functions employed are

$$N_i(\xi, \eta) = \tfrac{1}{4}(1 + \xi_i\xi)(1 + \eta_i\eta), \quad i = 1, \ldots, 4 \tag{1}$$

where (ξ_i, η_i) are the coordinates of the nodes. Using these shape functions and the Mindlin plate theory, the mass and stiffness element matrices are derived. The mass and stiffness element matrices for each element are assembled into the system

$$\boldsymbol{M}\ddot{x} + \boldsymbol{K}x = 0 \tag{2}$$

for degrees-of-freedom x, mass matrix $\boldsymbol{M}$ and stiffness matrix $\boldsymbol{K}$. The boundary conditions for the cantilever enforce zero deflection and rotation for each node along the clamped boundary. Non-trivial harmonic solutions $x(t) = u\cos(\omega t)$ for the above system satisfies the eigenvalue problem

$$\boldsymbol{K}u = \lambda\boldsymbol{M}u \quad (\lambda = \omega^2) \tag{3}$$

The matrices $\boldsymbol{K}$ and $\boldsymbol{M}$ are sparse allowing this eigenvalue problem to be solved using the Lanczos algorithm implemented in the software ARPACK. The numerical computations provide the modal frequency ω and if desired the mode shape u.

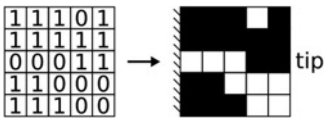

Fig. 1 *Binary matrix represents the topology of the cantilever. The clamped edge of the cantilever is on the left-hand side of the matrix and a set of elements are designated to be the tip of the cantilever*

3. Cantilever representation for optimisation: To design the cantilever, a fixed rectangular mesh is formed to denote the design space. Fixed sized elements are added or removed from the mesh. This allows the cantilever to be represented as a binary matrix as shown in Fig. 1. Each element represents a rectangular portion of the cantilever. If the element has a value of 1, the area is filled with material, if 0, it is void. The mesh used for the topology representation maps directly to the mesh used for FE analysis allowing for fast FE meshing and assembly.

The modification of the binary matrix during the optimisation routine does not guarantee that the resultant design features a cantilever topology. To ensure that the design is feasible before carrying out the FE analysis, an image processing routine [21] is applied to the cantilever topology.

A region identification routine is applied to the binary matrix to find all the separate structures in the topology. A region is deemed connected if it includes the tip and borders the clamped edge. Here, n_c is the number of connected regions and n_d is the number of disconnected regions. A feasible design must have $n_c = 1$ and $n_d = 0$. Elements with only one neighbouring element, denoted hinges, are discouraged. n_h is the number of hinges and $n_h = 0$ for a design to be feasible. Additional metrics A_d, the total area of the disconnect structures and A_m, the area of the smallest structure are generated for use in the optimisation.

In the example shown in Fig. 1, $n_c = 1$, $n_d = 1$, $n_h = 2$ and $A_d = A_m = 5$.

4. Optimisation with the genetic algorithm: The objective of the optimisation routine is to place the modal frequencies of the cantilever at integer multiples of the first modal frequency. To increase the speed of convergence, the optimisation routine is applied to a specified initial cantilever topology and moves its modal frequencies to the nearest integer multiple of the first.

The cantilever representation x is a binary matrix as described in Section 3. Since symmetry is enforced, x represents half of the cantilever and the full topology is generated for the image processing routine and FE analysis. The optimisation problem

$$\min \quad f(x) = \sum_{i=2}^{M} w_i\left(\frac{\lambda_i}{\lambda_1} - r_i^2\right)^2 \tag{4}$$

$$\text{s.t.} \quad x \in \Omega_f \tag{5}$$

seeks to minimise the error in modal frequency ratios while rejecting invalid designs. M is the number of modes to place, w_i are weights for each term in the cost function, λ_i are the eigenvalues of the cantilever FE model, r_i are the desired frequency ratios and Ω_f is the set of feasible cantilever designs.

The optimisation problem is a binary nonlinear weighted least-squares problem. The genetic algorithm was selected due to its natural affinity to operate on binary variables, ease at handling nonlinear cost functions, lack of requirement of the gradient of the cost function, ability to perform a global search and ability to enforce the feasible set of cantilever designs. Genetic algorithms have been applied in structural design to achieve objectives such as compliance minimisation and eigenfrequency maximisation [21–25].

The use of the genetic algorithm simplifies the optimisation routine compared with gradient-based-optimisation methods [15–17] previously applied to harmonic cantilever design. The stochastic nature of the genetic algorithm allows for a global search without the risk of converging to local minima and the only requirement of the cost function $f(x)$ is that it can be computed, no further analysis is required.

doi: 10.1049/mnl.2016.0586

```
1: procedure GENETIC ALGORITHM
2:     Generate cantilevers in the initial generation
3:     for each generation do
4:         Evaluate the fitness of each cantilever
5:         Select elite cantilevers for the next generation
6:         Select cantilevers for the crossover operator
7:         Crossover cantilevers to produce the next generation
8:         Mutate cantilevers resulting from the crossover operator
9:     end for
10: end procedure
```

Fig. 2 *The cantilever design genetic algorithm*

The optimisation problem is moved from a constrained to an unconstrained problem by applying a penalty to infeasible designs. The optimisation problem is restated with the cost function [21]

$$\min \quad F(x) = \begin{cases} f(x), & x \in \Omega_{\mathrm{f}} \\ f^* + \mathrm{viol}(x), & \text{otherwise} \end{cases} \tag{6}$$

where

$$\mathrm{viol}(x) = \Gamma_{\mathrm{d}} n_{\mathrm{d}} + \Gamma_a A_{\mathrm{d}} + \Gamma_m A_m + \Gamma_{\mathrm{h}} n_{\mathrm{h}} \tag{7}$$

f^* is a large constant to ensure all infeasible designs have a worst cost function than that of feasible designs and the parameters Γ_{d}, Γ_a, Γ_m and Γ_{h} are weighting values to penalise each undesirable metric in the violation function. The outline of the genetic algorithm is shown in Algorithm 1 (see Fig. 2). Many of the heuristics employed in the genetic algorithm are a result of the small size of the feasible set Ω_{f} compared with the full set of binary matrices.

The initial generation of cantilevers are all identical. This was deemed necessary as randomly generated structures tend to be infeasible. The mutation operator is necessary to create new designs in early generations. The genetic algorithm uses linear ranking to evaluate the fitness of each design. Rank-based fitness is particularly important due to the large penalty f^* given to infeasible designs. Elitism is employed to ensure the best designs are not lost. The parent cantilevers for the crossover operator are selected using the stochastic universal sampling. Uniform crossover is performed to produce the next generation of cantilevers. The mutation operator flips bits with a low probability. Mutation is only employed to non-void regions of the initial cantilever as the existence of material in large void regions of the binary matrix is highly likely to produce an infeasible design. The genetic algorithm is terminated after a fixed number of generations and the cantilever with the lowest cost function is selected.

5. Cantilever designs using optimisation: The initial cantilever design that is to be modified with the genetic algorithm is shown in Fig. 3*a*. The base section of this initial design is 400 µm long and 500 µm wide. The tip section is 400 µm long and 100 µm wide. Material properties used to model the cantilever are those of the silicon layer from the PiezoMUMPs microfabrication process provided by MEMSCAP [26]. Here, the thickness of the layer is 10 µm, the elastic modulus is 169 GPa, the density is 2500 kg m^{-3} and Poisson's ratio is 0.29. FEs that are used to form the topology are 10 µm long and 10 µm wide. The dimension of the FE model of the initial cantilever design is 7440.

Modal frequencies of the initial design are tabulated in Table 1(a) and the mode shapes are shown in Fig. 4. With this design, the frequency ratio setpoints r_i, introduced in (4), are chosen to be (3,4,8,13).

The genetic algorithm is applied to mutate the initial cantilever design. A population of 20 individuals is used for each generation, elitism moves 2 individuals to the next generation, uniform crossover swaps bits with a 50% probability and mutation flips bits with a 1% probability. The optimisation problem is executed for 500 generations in less than half an hour.

The first optimised cantilever design with a stiffness of 17.68 N m^{-1} is shown in Fig. 3*b*. From the FE modal analysis, the modal frequencies of the first optimised design are tabulated in Table 1 (b). Errors in the frequency ratios are smaller compared with the initial design and the frequency ratios of the cantilever have approached integer values. The checkerboard pattern results due to the binary matrix representation of the cantilever topology. The features size limit for the PiezoMUMPs microfabrication process is 2 µm; therefore, there is no difficulty etching the 10 µm square holes in the topology.

Self-actuation and self-sensing cantilevers provide great advantages in terms of robust Q control in tapping-mode AFM [27]. It

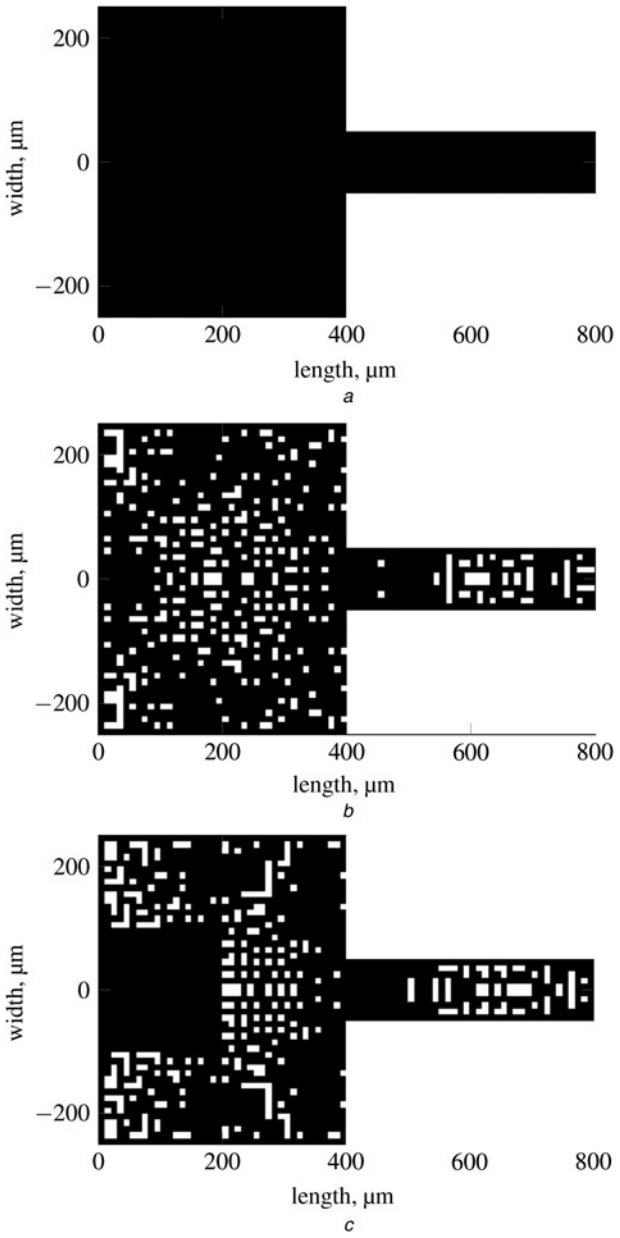

Fig. 3 *Initial cantilever design*
a Initial cantilever design that is modified with the genetic algorithm to move its modal frequencies down to integer multiples of the first modal frequency
b Execution of the genetic algorithm results in this first optimal cantilever design
c Modification was made where a large square area is preserved to allow for a piezoelectric layer to be added to the design

Table 1 From FE modal analysis, the modal frequencies of the initial cantilever and the two optimised cantilevers

Mode	Frequency, Hz	Ratio	Error, %	Type
(a) Modal frequencies of the initial design				
1	38,379	–	–	flexural
2	119,088	3.103	3.43	flexural
3	175,832	4.581	14.5	torsional
4	341,535	8.900	11.3	flexural
5	514,128	13.40	3.08	flexural
(b) Modal frequencies of the first optimised design				
1	35,860	–	–	flexural
2	107,093	2.986	0.47	flexural
3	143,833	4.010	0.25	torsional
4	287,127	8.006	0.08	flexural
5	466,294	13.00	0.00	flexural
(c) Modal frequencies of the second optimised design				
1	35,889	–	–	flexural
2	107,559	2.997	0.10	flexural
3	143,950	4.011	0.28	torsional
4	287,208	8.003	0.04	flexural
5	466,449	13.00	0.00	flexural

has the potential to reduce the physical size of an AFM by eliminating its optical components [28]. A piezoelectric layer is often laminated on the cantilever to serve as both actuator and sensor. In the first design proposed in this work, it is difficult to lay a piezoelectric layer on the cantilever due to its checkerboard pattern. As a result, modifications are made in the second design where an area is preserved to allow space for the piezoelectric layer. This is realised by preventing the mutation operator in the genetic algorithm from acting within this designated area. The resultant design is shown in Fig. 3*c*. The modal frequencies of the second design are shown in Table 1(c). Again, the frequency ratios lie close to integer values. The stiffness of the second optimised cantilever design is 17.77 N m^{-1}.

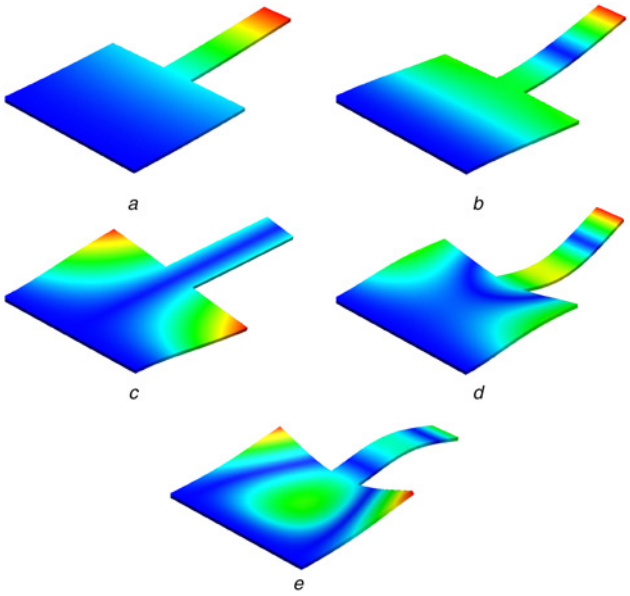

Fig. 4 *Cantilever modes of the initial cantilever topology from FE analysis*
a Mode 1 (flexural) 38.4 kHz
b Mode 2 (flexural) 119 kHz
c Mode 3 (torsional) 176 kHz
d Mode 4 (flexural) 342 kHz
e Mode 5 (flexural) 514 kHz

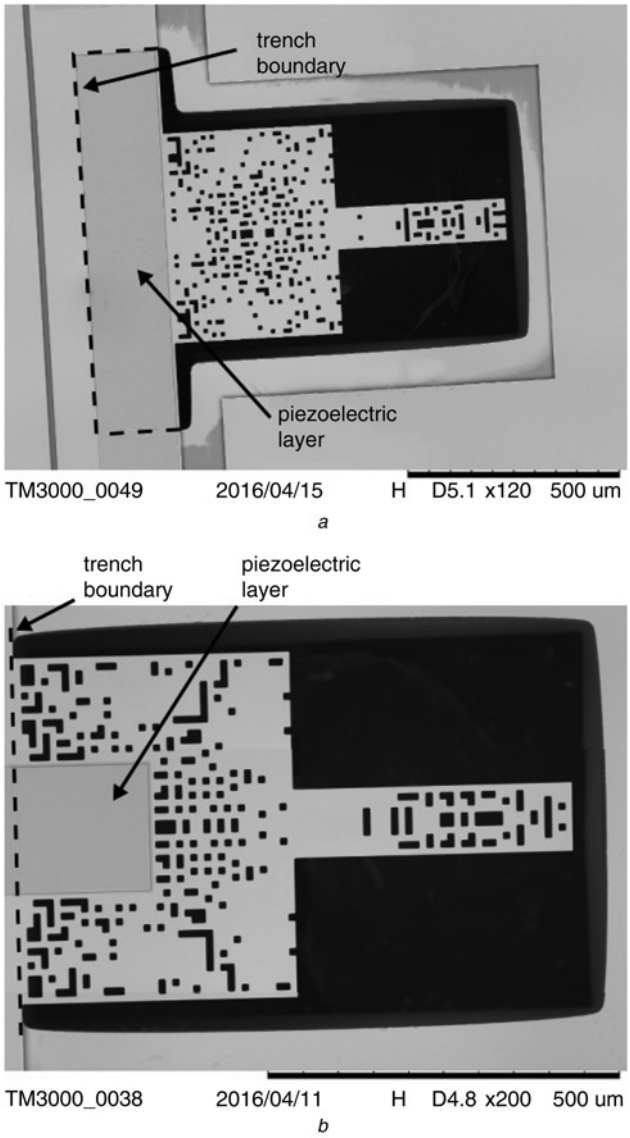

Fig. 5 *SEM images of the fabricated*
a First cantilever design
b Second cantilever design

6. Experimental characterisation: The cantilevers were fabricated with the PiezoMUMPs microfabrication process provided by the company MEMSCAP [26]. Fabrication starts with a double-sided silicon-on-insulator wafer. The top 10 µm layer of silicon is doped. A 0.2 µm oxide layer is grown and patterned with a reactive ion etch (RIE) to insulate the silicon layer. Next, a 0.5 µm piezoelectric layer of aluminium nitride is deposited and patterned with a wet etch. To provide electrical connections, a 1 µm layer of aluminium is deposited and patterned using a lift-off process. The device is then etched into the silicon layer using a deep RIE. Moreover, finally the device is released by etching through the bottom 400 µm silicon layer using multiple etching processes. A scanning electron microscope (SEM) (Hitachi TM3000) is used to image the fabricated cantilevers. The displacement of the cantilevers, for identification of the cantilever's frequency response, was measured using a laser Doppler vibrometer (Polytec MSA-400).

SEM images of the fabricated designs are shown in Fig. 5. To actuate the first cantilever design, the cantilever is appended to a large base as shown in Fig. 5*a*. A piezoelectric transducer is layered over the base plate to excite the cantilever. The area

doi: 10.1049/mnl.2016.0586

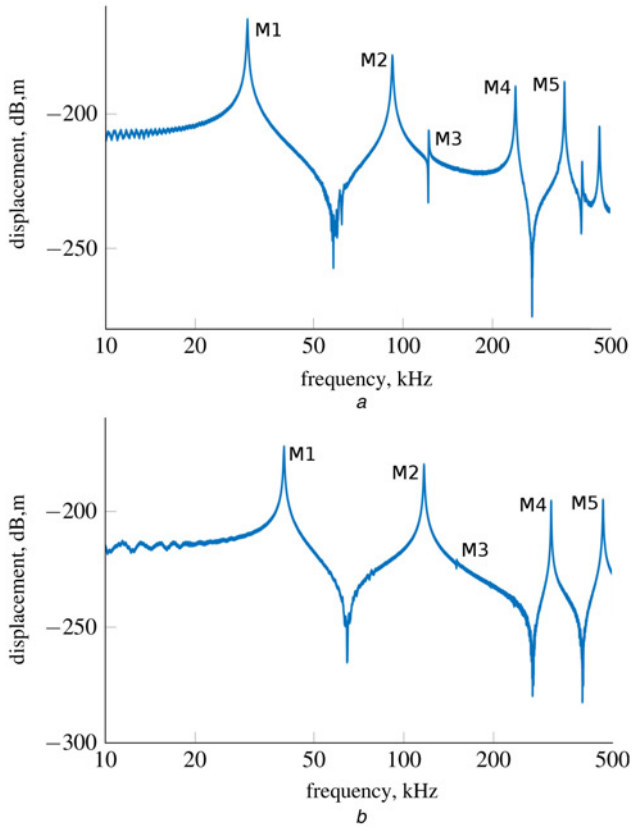

Fig. 6 *Magnitude response of the*
a First optimised cantilever design
b Second optimised cantilever design. The torsional mode (mode 3) may not be observable on this plot but is distinguishable with careful analysis of the measurements

under the cantilever and the base is trenched. As a result, three sides of the base, which are located at the edge of the trench, are fixed. It is assumed that the effect of the base on the cantilever's dynamics is negligible.

The purpose of the second optimised cantilever design was to allow space for a piezoelectric transducer on the cantilever. The SEM image in Fig. 5*b* shows the cantilever design with a piezoelectric layer in the designated rectangular space. The piezoelectric layer was assumed insignificant compared with the cantilever silicon layer due to its small thickness and area compared with the silicon layer. As a result, no modification of the FE model was made to account for the laminate structure formed by the piezoelectric layer.

Table 2 Experimentally determined modal frequencies and their ratios with respect to the fundamental frequency of the cantilever

Mode	Frequency, Hz	Ratio	Error, %
(a) Modal frequencies of the first cantilever design			
1	30,000	–	–
2	92,031	3.068	2.26
3	122,031	4.068	1.70
4	239,063	7.969	0.39
5	348,906	11.63	10.5
(b) Modal frequencies of the second cantilever design			
1	39,688	–	–
2	116,875	2.945	1.83
3	150,469	3.791	5.23
4	311,719	7.854	1.82
5	464,531	11.70	10.0

On both cantilevers, the piezoelectric transducer was excited with a 0.3 V periodic chirp. The displacement of the induced motion was measured at the end of the cantilever. The magnitude responses from voltage to displacement are shown in Fig. 6. The modes of the cantilevers can be seen clearly in the measured magnitude responses. The modes of the cantilevers were identified and their corresponding frequency, frequency ratio with respect to the first modal frequency and percentage error from the desired frequency ratio are tabulated in Table 2.

For the first cantilever design, the modal frequencies have decreased due to the presence of the base plate. Nevertheless, the frequency ratios are relatively precise for the second, third and fourth modes. Although ultimately to produce more accurate results, the base plate should be incorporated into the FE modelling. For the second cantilever design, the error in the mode 3 frequency ratio has increased compared with the first design. Here, the piezoelectric layer has had a significant effect. The largest frequency ratio error in both cantilevers is for mode 5. This is attributed to fabrication tolerances, in particular, the etching process of the trench area exhibits large dimensional variations, which is up to 50 µm in one direction [26]. This variation shifts the clamped boundary of the cantilever, which in turn changes its modal frequencies.

7. Conclusion: This work has outlined the design and characterisation of two harmonic cantilevers for multi-frequency AFM applications. These cantilevers amplify the harmonics produced during the nonlinear probe–sample interaction forces. Compared with previous harmonic cantilever designs, this work demonstrates a routine which is capable of placing several modal frequencies simultaneously at an integer multiples of the fundamental frequency. Furthermore, the routine is simple to implement and it can be used to place both torsional and flexural modes. It does not require the derivation/evaluation of gradients or differential equations. The discrete design variables provide for quick FE meshing.

The stochastic nature of the genetic algorithm is well suited to the design of harmonic cantilevers. The complex relationship between the parameters of the topology and its modal frequencies make the black box nature of the genetic algorithm ideal to perform a global search. Furthermore, no consideration of the optimisation algorithm is needed when parameterising the topology. The algorithm can handle additional design goals easily.

The experimental results show the accurate placement of modes 2–4 in the first cantilever design and modes 2 and 4 in the second cantilever design. Future work aims to account for fabrication and material property variances in the optimisation routine and include modelling the piezoelectric layer and AFM probe tip to improve the robustness and accuracy of the design routine.

8. References

[1] Wiesendanger R.: 'Scanning probe microscopy and spectroscopy' (Cambridge University Press, 1994)

[2] Yong Y.K., Moheimani S.O.R., Kenton B.J., *ET AL.*: 'Invited review article: high-speed flexure-guided nanopositioning: mechanical design and control issues', *Rev. Sci. Instrum.*, 2012, **83**, (12), p. 121101

[3] Devasia S., Eleftheriou E., Moheimani S.O.R.: 'A survey of control issues in nanopositioning', *IEEE Trans. Control Syst. Technol.*, 2007, **15**, (5), pp. 802–823

[4] Mazzeo A.D., Stein A.J., Trumper D.L., *ET AL.*: 'Atomic force microscope for accurate dimensional metrology', *Prec. Eng.*, 2009, **33**, (2), pp. 135–149

[5] Yamanaka K., Noguchi A., Tsuji T., *ET AL.*: 'Quantitative material characterization by ultrasonic AFM', *Surf. Interface Anal.*, 1999, **27**, pp. 600–606

[6] Choi K.-B., Lee J.J.: 'Passive compliant wafer stage for single-step nano-imprint lithography', *Rev. Sci. Instrum.*, 2005, **76**, p. 075106

[7] Sebastian A., Pantazi A., Moheimani S.O.R., *ET AL.*: 'Achieving sub-nanometer precision in a MEMS-based storage device during self-

servo write process', *IEEE Trans. Nanotechnol.*, 2008, **7**, (5), pp. 586–595
[8] Lozano J.R., Garcia R.: 'Theory of multifrequency atomic force microscopy', *Phys. Rev. Lett.*, 2008, **100**, (7)
[9] Garcia R., Herruzo E.T.: 'The emergence of multifrequency force microscopy', *Nat. Nanotechnol.*, 2012, **7**, (4), pp. 217–226
[10] Dietz C., Herruzo E.T., Lozano J.R., *ET AL.*: 'Nanomechanical coupling enables detection and imaging of 5 nm superparamagnetic particles in liquid', *Nanotechnology*, 2011, **22**, (12), p. 125708
[11] Garcia R., Proksch R.: 'Nanomechanical mapping of soft matter by bimodal force microscopy', *Eur. Polym. J.*, 2013, **49**, (8), pp. 1897–1906
[12] Sahin O., Yaralioglu G., Grow R., *ET AL.*: 'High-resolution imaging of elastic properties using harmonic cantilevers', *Sens. Actuators A, Phys.*, 2004, **114**, (23), p. 183190
[13] Sadewasser S., Villanueva G., Plaza J.A.: 'Modified atomic force microscopy cantilever design to facilitate access of higher modes of oscillation', *Rev. Sci. Instrum.*, 2006, **77**, (7), p. 073703
[14] Felts J.R., King W.P.: 'Mechanical design for tailoring the resonance harmonics of an atomic force microscope cantilever during tip–surface contact', *J. Micromech. Microeng.*, 2009, **19**, (11), p. 115008
[15] Xia Q., Zhou T., Wang M.Y., *ET AL.*: 'Shape and topology optimization for tailoring the ratio between two flexural eigenfrequencies of atomic force microscopy cantilever probe', *Front. Mech. Eng.*, 2014, **9**, (1), pp. 50–57
[16] Cai J., Xia Q., Luo Y., *ET AL.*: 'A variable-width harmonic probe for multifrequency atomic force microscopy', *Appl. Phys. Lett.*, 2015, **106**, (7), p. 071901
[17] Bharaj G., Levin D.I.W., Tompkin J., *ET AL.*: 'Computational design of metallophone contact sounds', *ACM Trans. Graph.*, 2015, **34**, (6), pp. 223:1–223:13
[18] Quek S.S., Liu G.R.: 'Finite element method: a practical course' (Elsevier Science, Burlington, USA, 1990)
[19] Ruppert M.G., Moheimani S.O.R.: 'Multimode Q control in tapping-mode AFM: enabling imaging on higher flexural eigenmodes', *IEEE Trans. Control Syst. Technol.*, 2016, **24**, (4), pp. 1149–1159
[20] Petyt M.: 'Introduction to finite element vibration analysis' (Cambridge University Press, Cambridge, UK, 1998)
[21] Wang S.Y., Tai K., Wang M.Y.: 'An enhanced genetic algorithm for structural topology optimization', *Int. J. Numer. Methods Eng.*, 2006, **65**, (1), pp. 18–44
[22] Jakiela M.J., Colin C., James D., *ET AL.*: 'Continuum structural topology design with genetic algorithms', *Comput. Methods Appl. Mech. Eng.*, 2000, **186**, (2-4), pp. 339–356
[23] Kim I.Y., deWeck O.L.: 'Variable chromosome length genetic algorithm for progressive refinement in topology optimization', *Struct. Multidiscip. Optim.*, 2005, **29**, (6), pp. 445–456
[24] Madeira J.F.A., Pina H.L., Rodrigues H.C.: 'GA topology optimization using random keys for tree encoding of structures', *Struct. Multidiscip. Optim.*, 2010, **40**, (1-6), pp. 227–240
[25] Garcia-Lopez N.P., Sanchez-Silva M., Medaglia A.L., *ET AL.*: 'An improved robust topology optimization approach using multiobjective evolutionary algorithms', *Comput. Struct.*, 2013, **125**, pp. 1–10
[26] Cowen A., Hames G., Konstantin G., *ET AL.*: 'PiezoMUMPs design handbook' (MEMSCAP Inc., 2014), vol. **1.3**
[27] Fairbairn M.W., Moheimani S.O.R., Fleming A.J.: 'Q control of an atomic force microscope microcantilever: a sensorless approach', *J. Microelectromech. Syst.*, 2011, **20**, (6), pp. 1372–1381
[28] Ruppert M.G., Moheimani S.O.R.: 'A novel self-sensing technique for tapping-mode atomic force microscopy', *Rev. Sci. Instrum.*, 2013, **84**, (12), p. 125006

doi: 10.1049/mnl.2016.0586